

2

**AD-A271 614**



**S**  
OCT 2 1993  
**D**

**FINAL REPORT**

to

**OFFICE OF NAVAL RESEARCH**

on

**LONG RANGE FAST TOOL SERVO**

**ONR CONTRACT NO. N00014-92-J-4082-PI**

Covering the period from June 1, 1992 to May 31, 1993

*Submitted by*

**G. McDonald Moorefield, II**  
Chief Engineer

**Karl J. Falter**  
Research Associate

**Thomas A. Dow**  
Professor  
Department of Mechanical & Aerospace  
Engineering

**Paul I. Ro**  
Assistant Professor  
Department of Mechanical & Aerospace  
Engineering

This document has been approved  
for public release and sale; its  
distribution is unlimited.

Precision Engineering Center  
North Carolina State University  
Raleigh, NC 27695-7918

**93-25510**



1998

93 10 21 083



### 3 AMPLIFIED-DISPLACEMENT ACTUATORS

After exhausting these direct-drive options, the search was directed toward amplified-displacement actuators such as bimorphs, levers, etc. These devices do provide significantly greater range, but in doing so, sacrifice open-loop stiffness and necessitate larger input forces (because of force de-amplification). Furthermore, with the lever design (where amplification is linearly dependent on the ratio of the output lever length to the input lever length), high amplifications can require prohibitively long output levers (in regard to space constraints as well as stiffness requirements). However, if the amplification mechanism is a function of an area ratio (e.g., hydraulic cylinders), high amplifications are possible without an unreasonable consumption of space or loss of stiffness. Because of its simplicity, compactness, and stiffness, a "closed-reservoir" hydraulic system (i.e., no circulating pump, no valves, etc., only two pistons sharing a common reservoir as shown in Figure 1) was selected for amplifying the motion of an input drive. Of course, because of the unavoidable force de-amplification (i.e., mechanical disadvantage), the input forces must still be large relative to the output forces.

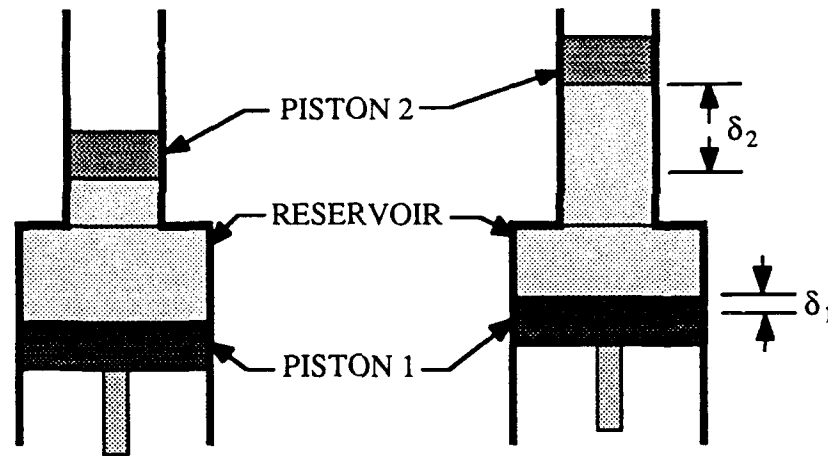


Figure 1: Area-Based Amplification with an Incompressible Fluid.

#### 3.1 Area-Based Displacement Amplification Using an Incompressible Fluid

A simple example of Area-Based (A-B) displacement amplification involves two pistons with different cross-sectional areas,  $A_1$  and  $A_2$ , sharing a common fluid reservoir (see Figure 1). For a perfectly incompressible (i.e., constant density) fluid, the reservoir volume will be conserved. Therefore, a quasistatic displacement  $\delta_1$  of Piston 1 will produce a displacement  $\delta_2$  of Piston 2 which is equal to the product of the input displacement and the ratio of the input area to the output area.

$$\Delta V = A_2 \delta_2 - A_1 \delta_1 = 0 \quad (1)$$

$$\delta_2 = \delta_1 \left( \frac{A_1}{A_2} \right) \quad (2)$$

### 3.2 Losses in A-B Displacement Amplifiers due to Fluid Compressibility

Unfortunately, all real fluids do exhibit some degree of compressibility. For many gases, especially those exhibiting nearly ideal gas behavior, density  $\rho$  is directly proportional to pressure  $P$  and inversely proportional to temperature  $T$ . Therefore, for air, compressibility is typically significant, especially in dynamic situations.

$$\rho \propto \frac{P}{T} \quad (3)$$

For liquids, density is much less dependent on pressure. A liquid's degree of compressibility can be expressed as "the ratio of the pressure stress to the volumetric strain," which is defined as the bulk modulus of elasticity  $B$

$$B = - \frac{v \Delta P}{\Delta v} \quad (4)$$

where  $v$  is the initial specific volume,  $\Delta P$  is the change in pressure, and  $\Delta v$  is the change in specific volume [4]. Bulk modulus values of pertinent liquids are shown in Table 1.

Type of Fluid	Bulk Modulus (psi)
Water	300,000 [5]
Water	294,000 [6]
Water at 25°C	346,000 [7]
Standard Hydraulic Fluid at 71°C	320,000 [8]
Standard Hydraulic Fluid at 25°C	250,000 [7]
Aircraft Synthetic (Phosphate Ester) at 71°C	308,000 [8]
Industrial Synthetic (Phosphate Ester) at 71°C	387,000 [8]
Synthetic (Phosphate Ester)	400,000 [6]
Silicate Ester at 71°C	196,000 [8]
Water-Glycol Mixture	385,000 [6]
Silicone Fluid	182,000 [9]
Mineral Oil	286,000 [6]
Chlorinated Hydrocarbon	417,000 [6]

Table 1: Bulk Moduli for Various Fluids.

Therefore, for maximum amplification, a hydraulic design was selected over a pneumatic design because, with the hydraulic design, less of the displacement of the input piston is spent compressing the exchange fluid. However, because the desired amplification is large, even hydraulic fluids can experience sufficient compression to significantly reduce the actual displacement of the output piston.

### 3.3 Estimating Compressibility Losses in A-B Displacement Amplifiers

Consider the system shown in Figure 2 where the fluid reservoir is initially pressurized by the input piston (driven by the force  $F_d$ ) and the spring-loaded output piston (restrained by the force  $F_s$  which is equal to  $K_s\delta_i$ , where  $K_s$  is the spring constant of the spring and  $\delta_i$  is the initial deflection of the spring). The fluid in the closed reservoir has an initial pressure  $P_i$ , an initial volume  $V_i$ , and an initial mass  $m_i$ . (For simplicity, the external pressure,  $P_{atm}$ , is assumed to be zero and body, normal, and friction forces on the pistons have been omitted.) Since the mass is constant for this closed system, Equation (4) can be rewritten in terms of volume (rather than specific volume) and rearranged to reveal that the reservoir capacity should be minimized to reduce the effects of the compressibility.

$$\Delta V = -\frac{V\Delta P}{E} \quad (5)$$

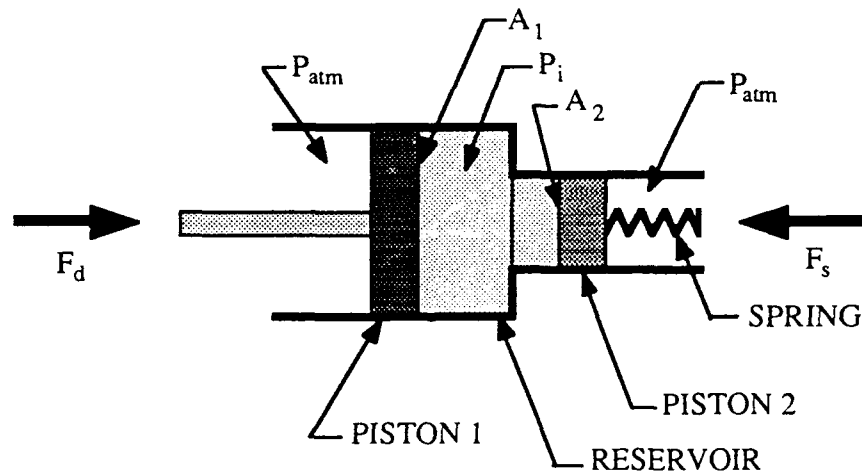


Figure 2: Area-Based Amplification with a Compressible Fluid.

The following equation can be obtained from the Initial Freebody Diagram of Piston 1 (see Figure 3a).

$$\sum F_x = F_d - P_i A_1 = 0 \quad (6)$$

The following equation can be obtained from the Initial Freebody Diagram of Piston 2 (see Figure 3b).

$$\sum F_x = P_i A_2 - F_s = P_i A_2 - K_s \delta_i = 0 \quad (7)$$

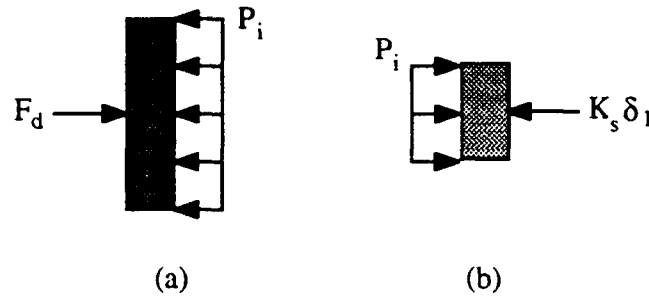


Figure 3: Initial Freebody Diagrams of (a) Piston 1 and (b) Piston 2.

Equations (6) and (7) can be rearranged to give the initial driving force

$$F_d = K_s \delta_i \left( \frac{A_1}{A_2} \right) \quad (8)$$

and the initial pressure.

$$P_i = \frac{K_s \delta_i}{A_2} \quad (9)$$

In the absence of external forces and neglecting inertial forces, quasistatically displacing the input piston by  $\delta_1$  would require the driving force  $F_d$  to increase by some amount  $\Delta F_d$  and would cause the retarding spring force  $F_s$  to increase by the amount  $K_s \delta_2$ , where  $\delta_2$  is the displacement of the output piston (which is also equal to the additional deflection of the spring). To satisfy the requirements for equilibrium, these increases in the forces applied to the pistons must increase the pressure of the fluid. The following equation can be obtained from the Final Freebody Diagram of Piston 1 (see Figure 4a).

$$\sum F_x = F_d + \Delta F_d - P_f A_1 = 0 \quad (10)$$

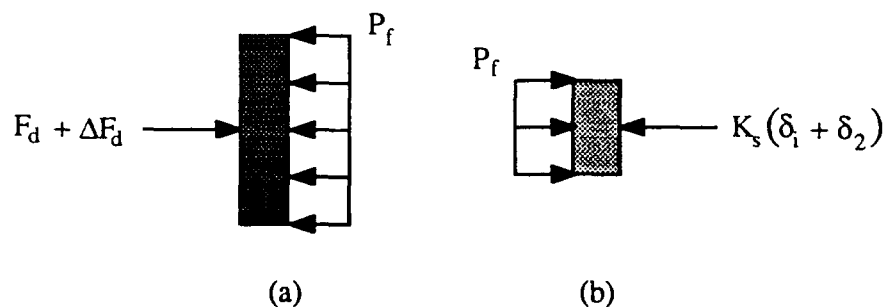


Figure 4: Final Freebody Diagrams of (a) Piston 1 and (b) Piston 2.

The following equation can be obtained from the Final Freebody Diagram of Piston 2 (see Figure 4b).

$$\sum F_x = P_f A_2 - F_s - \Delta F_s = P_f A_2 - K_s \delta_i - K_s \delta_2 = 0 \quad (11)$$

These equations can be rearranged to give the change in the driving force

$$\Delta F_d = K_s \delta_2 \left( \frac{A_1}{A_2} \right) \quad (12)$$

and the change in pressure.

$$\Delta P = \frac{K_s \delta_2}{A_2} \quad (13)$$

Substituting this expression for  $\Delta P$  into Equation (5) yields the decrease in the reservoir volume due to the increase in the fluid pressure.

$$\Delta V = - \frac{V K_s \delta_2}{E A_2} \quad (14)$$

After being modified for the case of a compressible liquid, Equation (1) can be incorporated into Equation (14) to give the following.

$$\Delta V = - \frac{V K_s \delta_2}{E A_2} = A_2 \delta_2 - A_1 \delta_1 \neq 0 \quad (15)$$

The actual output piston displacement  $\delta_2$  can now be calculated.

$$\delta_2 = \delta_1 \left( \frac{E A_1 A_2}{E A_2^2 + V K_s} \right) \quad (16)$$

Examination of Equation (16) reveals that the output displacement  $\delta_2$  will be maximized when the bulk modulus  $E$  and the input area  $A_1$  are maximized and the output area  $A_2$ , the initial volume  $V$ , and the spring constant  $K_s$  are minimized.

### 3.4 Losses in A-B Displacement Amplifiers due to Structural Deflections

Deflections of the actuator structure can potentially undermine the displacement amplification process due to the high forces and small displacements involved. Two potential problem areas are of particular significance: (1) the deflection of the structure supporting the input stack and (2) the distortions of the input piston and the fluid reservoir chamber. In both cases, the significant quantity is the change in deflection, not the absolute magnitude of the deflection (i.e., only the variations in the dynamic deflections are important; the static or preload deflections are irrelevant).

These deflections have the same net effect: a reduction in the volume of fluid displaced by the input piston and consequently a reduction in the output piston displacement necessary to accommodate the displaced fluid volume. For more on the analysis of the actuator prototype, please see Section 5.3.

## 4 TYPES OF PRIME MOVERS

For a large displacement amplification system, the prime mover, or input drive, will need only a modest range of extension, but must be capable of generating large forces because of the inherent mechanical disadvantage. In addition, the drive should be compact (in regard to both length and cross-section), stiff, and stable over a moderate range of temperatures. The input drive should be free from excessive hysteresis which could cause thermally-induced damage to the drive as well as dimensional instability in the actuator structure.

### 4.1 Electrostrictive Drives

Electrostriction is the occurrence of mechanical strain in a material when subjected to an electric field where "the deformation is independent of the direction of the field and proportional to the square of the field" [10]. The electrostrictive material Lead Magnesium Niobate (PMN) has less hysteresis, a higher elastic modulus, and less creep than a typical piezoelectric material, but its strain rate suffers from a severe dependence on temperature [10]. Although an elaborate cooling system could potentially eliminate this problem, the use of a piezoelectric material would likely be a better alternative.

### 4.2 Magnetostrictive Drives

Materials which exhibit the phenomenon of magnetomechanical strain (i.e., mechanical strain when subjected to a magnetic field) are called *magnetostrictive materials*. "Magnetostriction is a result of the rotation of small magnetic domains which causes internal strains in the material. These strains result in a positive expansion of [the magnetostrictive material] in the direction of a magnetic field. As the field is increased more domains rotate and become aligned until finally saturation is achieved, where nearly all domains are aligned in the direction of the field. If the field is reversed the domains reverse direction but again align along the field direction and also result in a length increase" [11].

Magnetostriction was first observed (in nickel) by James Joule in 1842 [12]. Until recently, magnetostrictive materials have been unable to challenge the strain rates attainable with piezoelectric materials; however, the development of Terfenol-D, the nearly single-crystal composition of Terbium, Iron, and Dysprosium, has made magnetostriction a viable alternative in many

applications [12,13]. Strain rates up to 2000 ppm have been reported for actuators using Terfenol-D [12,13].

Changing the magnetic field around a Terfenol-D rod produces a change in the length of the rod. Perhaps the most preferred mode of operation (because of improved linearity, minimal heating, etc.) is to use permanent magnets to induce a DC magnetic bias in the material, then to use an electrified coil to introduce the variable magnetic field which produces the mechanical strain [14].

The theoretical force capability  $F$  of a magnetostrictive actuator is given by the following equation

$$F = \frac{E A \Delta L}{L} \quad (17)$$

where  $E$  is the elastic modulus of the magnetostrictive material (35 MPa for Terfenol-D),  $A$  is the cross-sectional area of the magnetostrictive element,  $\Delta L$  is the elongation of the element, and  $L$  is the length of the element [13,15]. However, a Terfenol-D actuator's practical force capability is significantly lower due to the reduction in strain rate associated with high actuator loads [15]. See Table 2.

### 4.3 Piezoelectric Drives

Piezoelectric behavior is defined as the ability of a material to produce an electrical charge when subjected to an external force or pressure (the term "piezo" originates from the Greek word meaning pressure) [16]. Piezoelectric materials also possess the ability to produce mechanical strain when subjected to an electric field where the strain is directly proportional to the electric field. These effects - the piezo effect and the "inverse piezo" effect - were observed in quartz by Jacques and Pierre Curie in the late nineteenth century [16]. The piezo effect in a single crystal is due to the mechanically-forced alignment of the dipoles within the unit cells; the inverse piezo effect in a single crystal is due to the electrically-induced alignment of the dipoles within the unit cells [17].

Ferroelectrics, a subclass of piezoelectrics, are polycrystalline materials composed of dipole domains and exhibit a remanent, or residual net, polarization after the electric field is removed because of dipole coupling (i.e., the alignment of one dipole affects the alignments of the neighboring dipoles) [18]. Ferroelectrics can achieve significantly greater strain than single crystal piezoelectrics because the strain "is in fact a sum of strain piezoelectrically produced in individual domains and strain caused by rotation of 90°-domains" [19].

The electric field  $\xi$  (i.e., the voltage per unit distance) generated by a piezoelectric material when stressed is given by the relationship

$$\xi = g \sigma \quad (18)$$

where  $\sigma$  is the applied stress and  $g$  is a constant [18]. The mechanical strain  $\epsilon$  experienced by a piezoelectric material when subjected to an electric field is given by the following relationship

$$\epsilon = d \xi \quad (19)$$

where  $\xi$  is the applied electric field and  $d$  is a constant [18]. The two constants  $g$  and  $d$  (0.145 V-m/N and 0.25 nm/V, respectively, for Lead Zirconate Titanate) are related to each other by the following expression

$$E = \frac{1}{d g} \quad (20)$$

where  $E$  is the elastic modulus [18].

The theoretical force capability (also known as the blocking force or stall force) of a PZT actuator is also given by Equation (17) [20,21]. Unlike magnetostrictive materials, constant loads below a PZT stack's stall force usually pose no real problems [20]. However, if the displacement of the piezoelectric stack is opposed by a force which increases with increases in displacement (i.e., a spring), the actual displacement will be less than the theoretical displacement [20]. The maximum extension of the stack is reduced according to the following relationship

$$\delta_{l_{actual}} = \delta_l \left( \frac{K_{pzt}}{K_{pzt} + K_s} \right) \quad (21)$$

where  $K_{pzt}$  is the stiffness of the piezoelectric stack and  $K_s$  is the stiffness of the driven system [20].

Type of Drive	Typ. Strain ( $\mu\text{m}/\text{mm}$ )	Force Capability (N)	Elastic Modulus (GPa)
<b>Electrostrictive:</b> Stack composed of Lead Magnesium Niobate wafers (6 mm diameter x approximately 150 $\mu\text{m}$ thick) and electrodes	0.8 [22]	700 [22]	110 [22]
<b>Magnetostrictive:</b> Rod composed of Terfenol-D (6.35 mm diameter)	1.0 [13]	220-330 [13]	35 [13]
<b>Piezoelectric (Ferroelectric):</b> Stack composed of Lead Zirconate Titanate wafers (6.35 mm diameter x 0.508 mm thick) and electrodes	1.1 [21]	960 [21]	27 [21]

Table 2: Comparison of Electrostrictive, Magnetostrictive and Piezoelectric Drives.

Because of its high strain rate, large force capability, and compactness as a drive, the ferroelectric material Lead Zirconate Titanate (PZT) appears to be best-suited for this high-force application. Therefore, if A-B amplification could be successfully implemented, a ferroelectric stack of modest length (e.g., 30 mm) and cross-sectional area (e.g., 660 mm<sup>2</sup>) could provide a small input displacement (25-30 μm) which would be amplified to obtain the desired output displacement (1 mm).

## 5 PROTOTYPE DESIGN OF A PIEZOELECTRIC/HYDRAULIC ACTUATOR

An actuator prototype was designed to test the feasibility of a piezoelectrically driven, hydraulically amplified actuator to provide precision motion over a one (1) mm range. Other applications such as Toyota's dynamically variable damping shock-absorber (called Piezo-TEMS - Toyota Electronically Modulated Suspension) [23] and Kinetic Systems' piezoelectric/hydraulic fuel injector with 15:1 displacement amplification [24] have benefited from the successful implementation of similar designs.

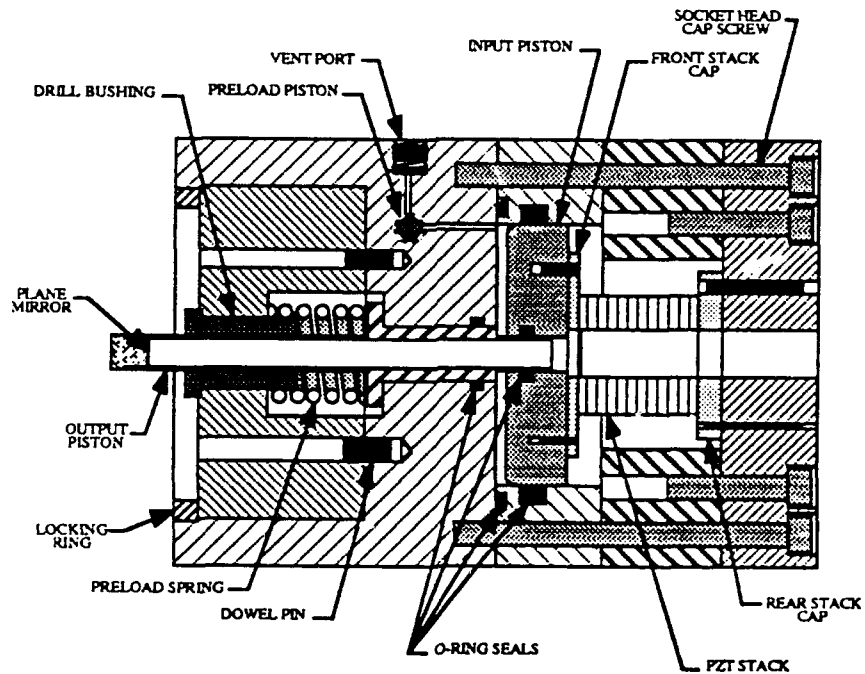


Figure 5: Long Range Actuator Prototype (section view, half size).

## 5.1 Prototype Design

The actuator (shown in Figure 5) consists primarily of a housing, an input piston driven by a piezoelectric stack, an output piston restrained by a coil spring, and a screw-driven preload piston. The housing is constructed of mild steel and includes the input, output, and preload pistons. The input piston is bolted to the stack which is, in turn, bolted to the housing endcap. The 25  $\mu\text{m}$  stroke input piston has an annular area of 3761  $\text{mm}^2$ , is sealed with o-rings, and has no guides or bearings. The one (1) mm stroke output piston is hollow, has an annular area of 88  $\text{mm}^2$ , is sealed with o-rings, and uses a bushing to guide its motion. (In the final actuator design, flexures will be used to guide the motion of the output piston.)

## 5.2 Prototype Operation

The actuator motion is generated by a piezoelectric stack. The stack is supplied a voltage which is nominally proportional to the desired displacement of the input piston (which is approximately one fortieth of the desired output piston displacement). The applied voltage forces the stack to mechanically strain. Since the stack is constrained at the rear end, it must lengthen toward the front of the actuator (i.e., the output end). As the stack lengthens, the input piston displaces a small volume of the reservoir fluid. The displaced volume (less the volume lost to fluid compression and mechanical deflections) forces the output piston toward the front of the actuator against the retarding force of the preload spring. Because of the ratio of the input area to the output area, the output piston is displaced approximately forty (40) times the input displacement. When the voltage is removed, the stack length decreases and the input piston retracts. The preload spring drives the output piston back, keeping the fluid forced against the input piston. To compensate for hysteresis, closed-loop control of the actuator is implemented via laser interferometer position feedback. The laser interferometer (located on a free-standing mount behind the actuator) detects the motion of the output piston by probing the plane mirror surface mounted inside the output piston.

## 5.3 Analysis of Prototype Design

As stated earlier, the deflection of the actuator is largely due to the compression of the acting fluid and the distortion of the fluid cavity. Simple spreadsheet calculations reveal the theoretical compression of the fluid to be less than 0.1%, but the stiffness of the actuator and the distortion of the fluid chamber are difficult to determine. It was because of this complexity that finite element analysis proved particularly invaluable. The finite element analysis package used was ANSYS® by Swanson Analysis Systems, Inc. An axisymmetric model was used (although the actual structure is not completely axisymmetric) to provide conservative results while limiting the size of the model. The reservoir fluid was modeled using hydrostatic fluid elements.

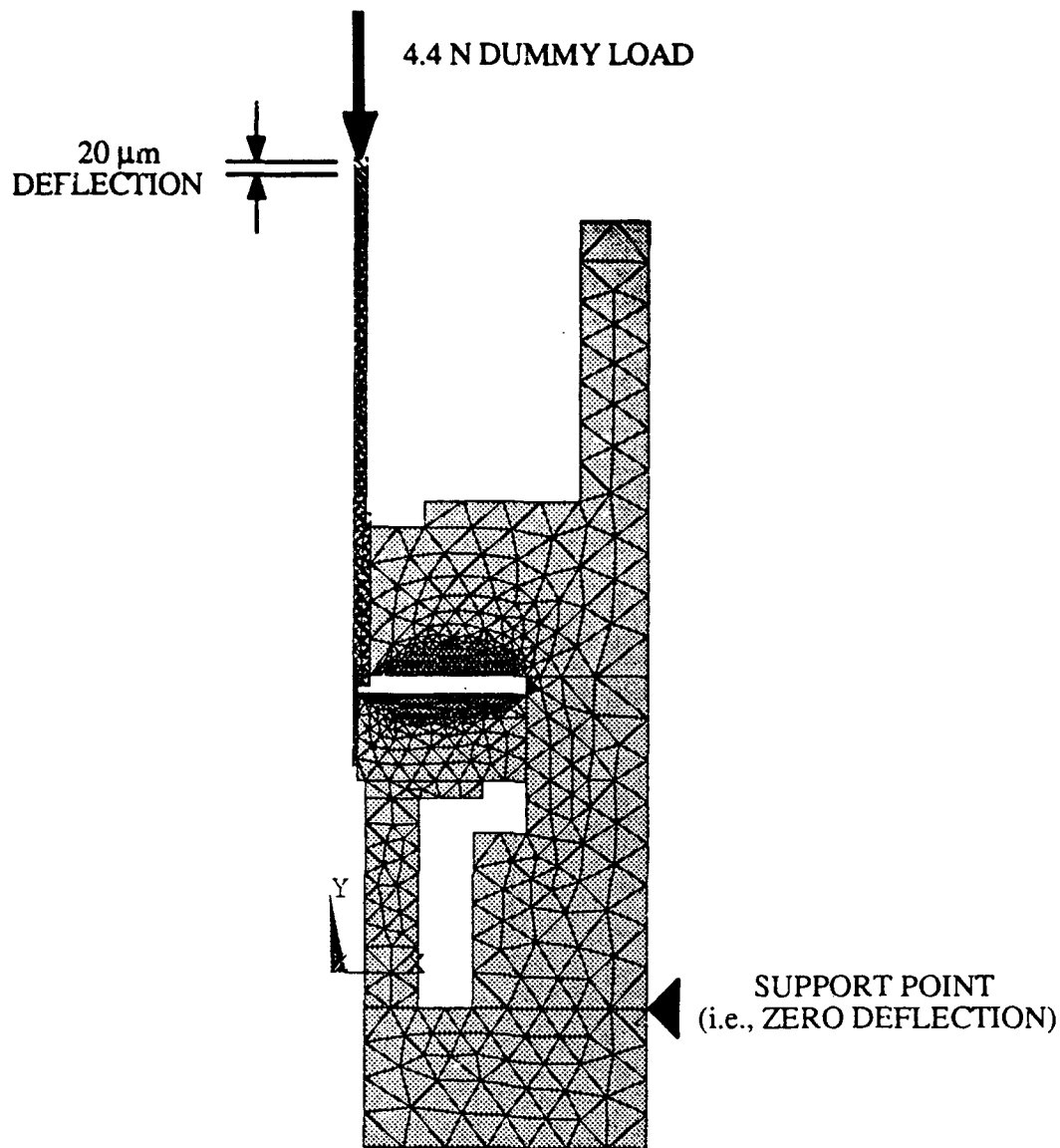


**Figure 6:** Finite Element Analysis Model of Prototype (using the revolution of an axisymmetric section). Note that the structure which guides the motion of the output piston contributes little to the stiffness of the actuator and has been omitted from this model.

By imposing an arbitrary load on the output piston, an overall, open-loop, actuator stiffness of  $0.22 \text{ N}/\mu\text{m}$  was computed. (See Figure 6.) That is, when the dummy load is applied, the output piston compresses the fluid and the fluid transmits the pressure to the walls of the chamber, causing the walls to deflect. The deflection of the walls and input piston increase the volume of the chamber and allow the output piston to further deflect. The model using the hydrostatic fluid elements accounts for all of this activity and directly yields the resultant deflection of the output piston, thereby eliminating time-consuming, potentially difficult calculations. If the hydrostatic elements had not been available, it would have been necessary to calculate the pressure due to the dummy load and then apply this pressure to the walls in the model to find the deflection of the

chamber walls. Using these geometrically complicated deflections, the increase in chamber volume would be calculated and the deflection of the output piston (due to the chamber distortion) would finally be computed.

Finite element analysis was also used to determine the structural dimensions necessary to produce sufficiently small deflections when subjected to the expected input forces and reservoir pressures. In modeling earlier versions of the actuator it was found that the fluid chamber had good rigidity, but the input piston experienced considerable deflection. Furthermore, the plate supporting the piezoelectric stack suffered excessive deflections, causing wasted motion of the stack. Subsequent design revisions reinforced these elements and improved the overall stiffness of the actuator.

A more detailed, non-axisymmetric model was also created to analyze the bolted joints within the actuator assembly. (Since the actuator has planes of symmetry it was possible to model a section comprising only an eighth of the structure.) It was found that the original design did not have enough bolts to guarantee a rigid structure. It was also discovered that over-tightening the bolts could distort the interface between the elements of the structure, thereby reducing the interface stiffnesses and creating the potential for fluid leaks (since the interface surfaces would not be completely contacting).

#### 5.4 Prototype Setup

To assemble the actuator, the output piston is inserted into its bore first. The coil spring is slipped onto the shaft of the output piston. Next, when the bushing subassembly is slipped over the output piston and mounted to the housing, the coil spring displaces the output piston toward the rear of the actuator until the flange on the output piston bottoms against the front face of the output piston bore. Then the reservoir is filled with a 50-50 mixture of water and ethylene glycol and the input piston is inserted into its bore, causing the entrapped air and excess fluid to be driven out the vent port on the top of the actuator. The vent port is closed, the assembly is bolted together, and the reservoir is brought to the minimum operating pressure by screwing the preload piston inward. This initial pressure in the reservoir forces the output piston forward against the force of the spring, moving the output piston's flange off the front face of the output piston bore. The product of the spring constant and the spring deflection at the output piston's initial equilibrium position gives the preload force on the output piston.

The amount of preload force required was calculated based on the moving mass at the maximum amplitude and frequency. For this actuator design, the output piston was considered the moving mass and was approximated as 100 g. However, when this prototype is modified to function as a tool positioning servo, the moving mass will also include the mass of the tool, the tool holder, and flexure clamping hardware. For that reason, 450 g was used as the design mass. The acceleration of an object experiencing sinusoidal oscillation is given by the equation

$$\ddot{Z} = -Z \omega^2 \sin(\omega t) \quad (22)$$

where  $\ddot{Z}$  is the acceleration,  $Z$  is the oscillation amplitude,  $\omega$  is the oscillation frequency (in radians per second), and  $t$  is time. Using the following equation and assuming a 500  $\mu\text{m}$  amplitude, 50 Hz sine wave, the maximum acceleration  $\ddot{Z}_{max}$  was estimated to be approximately 50  $\text{m}/\text{sec}^2$ .

$$\ddot{Z}_{max} = -Z \omega^2 \quad (23)$$

Using the mass and acceleration values and a very conservative factor of safety of four (4), the minimum preload force was set at 90 N. For a spring constant of 25 N/mm, the initial deflection should be 3.6 mm.

### 5.5 Piezoelectric Stack

A hollow piezoelectric stack is used to drive the actuator. The annular stack design provides better dissipation of the stack's hysteretic heat and allows the laser interferometer system access to the plane mirror surface on the output piston. The stack, manufactured by Kinetic Systems, has a 31.75 mm outside diameter and a 12.7 mm inside diameter. The stack consists of fifty-six (56) active 0.508 mm thick lead zirconate titanate (PZWT100) discs alternating with beryllium copper electrodes. A stack is assembled by laminating the required numbers of discs and electrodes with epoxy, and then encapsulating the assembly in a thin layer of epoxy. An inactive disc is located at each end of the stack to electrically insulate the stack from the two steel endcaps. The stack surfaces (i.e., the outer surfaces of the steel endcaps) are ground to provide parallel mounting surfaces. To protect the brittle stack material from potentially destructive tensile stresses, the fluid reservoir is initially pressurized to provide a preload force on the input piston. The design preload force is approximately 3800 N. The maximum force on the stack (occurring when the stack has reached its maximum elongation at a frequency of 50 Hz) should not exceed 6800 N.

Typically, the odd-numbered electrodes are all connected in parallel to one amplifier lead and the even-numbered electrodes are all connected in parallel to other amplifier lead. The numbers of discs and electrodes are determined by the desired range of motion (i.e., the mechanical strain within the stack). When a voltage is applied across the stack leads, the positive and negative electrodes subject the PZT discs to an electric field. The electric field causes the dipoles in the disc material to rotate, thereby producing elongation of the disc. Because of hysteresis within the disc material, heat is generated. For stacks operating with high field strengths (i.e., voltage per disc thickness ratios of 1.4  $\text{V}/\mu\text{m}$  or greater), the generated heat can be sufficient to cause the epoxy to out-gas, thereby compromising the stack's insulation and introducing the risk of stack delamination.

To prevent catastrophic failure of the stack, the heat generated must be removed from the surfaces of the stack at a rate equal to the heat generation within the stack. To provide the required heat transfer, the stack's surface area is maximized and compressed air flow is used to supplement conduction and natural convection. An important consideration is that the actual rate of heat transfer from the stack surfaces may be limited by the rate of conduction through the stack itself. To permit the required rate of conduction and thereby prevent dangerously high internal temperatures, the use of a high thermal conductivity epoxy is essential.

For stacks operating with high field strengths, heat is generated according to the equation

$$Q = 2.62 \times 10^{-6} n V f E^{2.86} \quad (24)$$

where  $Q$  is the heat generated (in watts),  $n$  is the number of discs,  $V$  is the volume of one disc (in  $\text{mm}^3$ ),  $f$  is the operating frequency (in Hertz), and  $E$  is the electric field strength (in volts per  $\mu\text{m}$  of disc thickness) [21]. For this stack, the amount of heat generated for 25  $\mu\text{m}$  displacement, 50 Hz operation was estimated to be 10 watts.

## 5.6 Position Feedback

Laser interferometer position feedback is used in the closed-loop control of the actuator. To isolate the position-sensing system from the distortions of the actuator housing, the laser interferometer is located on a free-standing mount behind the actuator. The system is configured as a single-pass, plane mirror interferometer (see Figure 7) with a resolution of 2.5 nm.

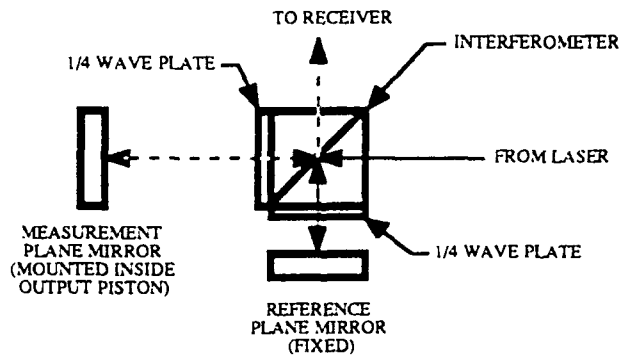


Figure 7: Laser Interferometer Schematic.

The Helium-Neon laser light enters the interferometer from the rear port. Inside the interferometer, the light is separated into the reference and measurement beams. The reference beam exits the interferometer, passes through a quarter-wave plate, strikes the stationary plane mirror and is directed back through the quarter-wave plate and into the interferometer. The measurement beam

exits the interferometer, passes through a quarter-wave plate, passes through the access hole in the actuator's endplate, through the central hole of the PZT stack, and through the hollow output piston until it strikes the plane mirror surface (mounted inside the output piston). The mirror reflects the beam back through the actuator, through the quarter-wave plate, and into the interferometer. The reference and measurement beams recombine inside the interferometer, exit through the side port, and are collected by the receiver.

## 6 PROTOTYPE PERFORMANCE TEST

The actuator prototype has been fabricated and assembled, and initial testing has begun. Preliminary results indicate that the 40X amplification in displacement can be obtained: 1000 VDC applied to the PZT stack produced approximately one (1) mm of displacement of the output piston (as measured with a mechanical indicator). However, the motion of the output piston was neither smooth nor reversible. Possible causes of this behavior include friction or binding in the guide bushing, o-ring friction, and compression of residual air in the fluid reservoir. After removing the guide bushing and minimizing the opportunity for air entrapment, tests revealed a nonlinear output piston displacement (i.e., a rapid initial displacement was followed by a slow drift in position) which strongly suggested the presence of o-ring creep. Another possible cause for the drift in output piston displacement could be drift (or creep) in the straining of the PZT stack. However, this drift in the output piston displacement was still observed after the PZT stack was replaced with a screw drive. Also observed in this test was drift in the position of the input piston (as measured with an electronic indicator) which suggested that o-ring creep was also influencing the motion of the input piston.

## 7 FUTURE WORK

The overall stiffness of the actuator will be measured (by measuring the static deflection of the output piston when loaded with a calibrated load) and compared to the 220 N/mm stiffness predicted by the finite element model. Also, open-loop dynamic performance tests will be performed for various displacement amplitudes and frequencies. Based on the results of the prototype performance test, the prototype design will be refined and modified to act as a fast tool servo actuator. Modifications may include the following: the implementation of guide flexures, alternative sealing systems, and high specific stiffness materials for the fabrication of the input and output pistons. Keys to success will be (1) the elimination of or compensation for the drift in the output piston displacement, (2) the minimization of the output piston/tool holder mass, (3) the proper characterization of the actuator's dynamics, (4) the integration of a 1000 VDC, 0.5 ampere amplifier, and (5) the implementation of high-speed, real-time control.

## REFERENCES

- [1] Garrard, K. P., Moorefield, II, G. M., and Taylor, L. W., "MAC 100 Fast Tool Servo", *Precision Engineering Center 1992 Annual Report, Volume X*, Precision Engineering Center, North Carolina State University.
- [2] Gerchman, M. C., "A Description of Off-Axis Conic Surfaces for Non-Axisymmetric Surface Generation", Submitted for presentation at ECO3 - International Congress on Optical Science & Engineering, The Hague, The Netherlands, *SPIE Proceedings Vol. 1266*, March 15, 1990.
- [3] Luttrell, D. E. and Dow, T. A., "Design of a Constant Velocity Micro-Stepping Actuator", *Precision Engineering Annual Report 1987, Volume V*, Precision Engineering Center, North Carolina State University.
- [4] Avallone, Eugene A. and Baumeister, Theodore, III, Marks' Standard Handbook for Mechanical Engineers, p. 3-36, 9th ed., McGraw-Hill, 1978.
- [5] Sullivan, James A., Fluid Power: Theory & Application, Reston Publishing Co., 1982.
- [6] Warring, R. H., Hydraulic Handbook, 8th ed., Gulf Publishing Co., Book Division, 1983.
- [7] Guillon, M., Hydraulic Servo Systems: Analysis and Design, Butterworths, 1969.
- [8] Keller, George R., Hydraulic System Analysis, 3rd ed., Published by the Editors of Hydraulics & Pneumatics Magazine, 1978.
- [9] Yeaple, F. D., Hydraulic and Pneumatic Power and Control: Design, Performance, Application, McGraw-Hill, 1966.
- [10] Cady, W. G., Piezoelectricity, pp. 198-199, First Edition, McGraw-Hill, 1946.
- [11] Butler, J. L., "Application Manual for the Design of ETREMA Terfenol-D Magnetostrictive Transducers", available through ETREMA Products, Inc., Ames, Iowa 50010.
- [12] Wang, Wanjun and Busch-Vishniac, Ilene, "A high precision micropositioner based on magnetostriction principle", *Rev. Sci. Instrum.* (American Institute of Physics), Vol. 63, No. 1, January 1992.

- [13] Goodfriend, M. J., "Material Breakthrough Spurs Actuator Design", Machine Design, Penton Publishing, March 21, 1991.
- [14] Bryant, M. D., "The Feasibility of Using Magnetostrictive Terfenol as a Precise Actuator", *Third Annual Report on Precision Engineering - SRO 154* (ONR Contract No. N00014-83-K-0064), Precision Engineering Laboratory, North Carolina State University, Jan., 1986.
- [15] Goodfriend, M. J., Shoop, K. M., and Miller, C. G., "High force, high strain, wide band width linear actuator using the magnetostrictive material, Terfenol-D", available through ETREMA Products, Inc., Ames, Iowa 50010.
- [16] Vorndran, S. and Hardwick, D., "Micropositioning with Piezoelectric Actuators", Motion Control, May, 1993.
- [17] Flinn, R. A. and Trojan, P. K., Engineering Materials and Their Applications, pp. 618,619 & 622, Second Edition, Houghton Mifflin Co., 1981.
- [18] Askeland, D. R., The Science and Engineering of Materials, pp. 603-606, Brooks/Cole Engineering Division, 1984.
- [19] Ikeda, T., Fundamentals of Piezoelectricity, pp. 177-178, Oxford University Press, 1990.
- [20] Products for MicroPositioning (Catalog, CAT 107-05/90.12), Physik Instrumente.
- [21] O'Neill, C.G., Kinetic Systems, Facsimile Transmission, July 31, 1991.
- [22] Rawal, B. and Galvagni, J., "Solid State Actuators Provide Micron-Level Displacement", Motion Control, January, 1992.
- [23] Simanaitis, D., "Tech Notes: M. Blaise Pascal and Toyota-San team up", Road & Track, July, 1990.
- [24] O'Neill, C.G., Kinetic Systems, Facsimile Transmission, July 14, 1993.